Critical radius for exchange bias in naturally oxidized Fe nanoparticles

C. Martínez-Boubeta, K. Simeonidis, and M. Angelakeris
Department of Physics, Aristotle University of Thessaloniki, 54124 Thessaloniki, Greece

N. Pazos-Pérez and M. Giersig
CAESAR, Department of Nanoparticle Technology, Ludwig-Erhard-Allee, D-53175 Bonn, Germany

A. Delimitis and L. Nalbandian
Chemical Process Engineering Research Institute, P.O. Box 361, 57001 Thessaloniki, Greece

V. Alexandrakis and D. Niarchos
Institute of Materials Science, NCSR Demokritos, 15310 Athens, Greece
(Received 4 April 2006; revised manuscript received 9 June 2006; published 28 August 2006)

Details of synthesis and structural characterization of highly crystalline iron oxide nanoparticles are presented together with results on the magnetic investigation as a function of the temperature and applied field. Monodisperse Fe nanoparticles were prepared by thermal decomposition of iron pentacarbonyl in the presence of oleic acid. These iron nanoparticles were readily oxidized on exposure to air. The resulting nanocrystals have been identified as inverse spinels, being γ-Fe_2O_3 the dominant phase of the small 5-nm iron oxide nanocrystals, whereas the proportion of the Fe_3O_4 component gradually increases on increasing the particle size. The small particles volume resulted in finite-size effects, for instance, the magnetization deviates from the $T^{3/2}$ Bloch's law. At the same time, high field irreversibility and shifted hysteresis loops after field-cooled processes have been detected, and attributed to a low-temperature surface spin-glass layer. Moreover, there is a critical diameter below which the surface spin-glass behavior and exchange bias effect abruptly disappear.

DOI: 10.1103/PhysRevB.74.054430 PACS number(s): 75.20.−g, 61.46.−w, 75.50.Bb, 75.50.Tt

I. INTRODUCTION

The "feedback" of technological society has strained an intense research in the past three decades on nanoscale particles (NPs). It is strongly believed that understanding the unique properties of small magnetic entities, in many cases arising from the high surface-to-volume ratio, would lead to novelty applications in medical imaging and drug targeting, cancer treatment through hyperthermia, catalysis, biological labeling, refrigeration systems, painting, archaeology dating, as well as an improved performance in magnetic recording media and permanent magnets.[1]

Regarding the magnetic features, below a critical size the magnetic entities become single domain and the magnetization reversal, assuming coherent rotation (of the magnetic domain moment), is well described within the Stoner-Wolhfarth model.[2] In addition, it was shown by Néel that at temperatures above the so-called blocking temperature T_B a stable bulk magnetization cannot be established due to thermal fluctuations.[3] The magnetic anisotropy energy that stabilizes the magnetization of a particle in a certain direction is generally proportional to the particle volume. At a certain temperature, there is a critical size below which the particle magnetic moment starts to fluctuate and goes through a rapid superparamagnetic relaxation and zero coercive field. Therefore the truly exciting fact about the magnetic properties of NPs, related to applications, is that they can exhibit size-dependent features [i.e., the lowest (zero) or the highest attainable coercivity]. For instance, high coercivity is critical on magnetic recording media, whereas very low coercivity is desirable in transformer core materials.

Another important magnetic issue in magnetic NPs analysis is the spin configuration. Frequently, the surface region of nanostructured magnetic matter exhibits modified magnetic properties compared to bulk as a consequence of the lack of structural periodicity and/or the presence of competing magnetic interactions, resulting in a noncollinear spin configuration, or spin canting, at the particle surface, and reduced saturation magnetization M_s.[4] Therefore interface effects dominate leading to a multiphase character, with phases magnetically and/or structurally different, which are modulated on the nanometer length scale. Actually such phases do interact, giving rise to intraparticle exchange anisotropy, as found in both oxide particles[5] and metallic systems.[6] The simulation of such magnetic behavior, based on a model of a magnetic core surrounded by a shell with spin disorder, is generally in good agreement with the experiments.[7] Furthermore, the exchange interaction has been shown to provide additional anisotropy energy to stabilize the magnetization of a nanoparticle and consequently may prevent the superparamagnetic limit during miniaturization.[8]

For the economical production of large quantities of NPs, milling is difficult to compete with. However, the product tends to be very polydisperse in size and irregular in shape that hinders the physical properties from being characterized. Solution chemistry approaches, either in aqueous or in organic solvents, have also been used to synthesize extremely small and almost monosized iron-based nanoclusters.[1] In this paper, crystalline magnetic oxides were obtained from colloidal dispersions of iron prepared by a process similar to that described in Ref. 9. We present the results of dc magnetic properties with respect to temperature and magnetic field, showing evidence of the existence of the surface spin-glass behavior in ionic magnetic solids above a critical diameter.

II. EXPERIMENT

Monodisperse Fe NPs were prepared via thermal decomposition of iron pentacarbonyl $Fe(CO)_5$. In a typical homogeneous nucleation synthesis, for instance, to prepare 11 -nm particles, 0.2 mL of $Fe(CO)_5$ (1.52 mmol) was added to a mixture containing 10 mL of octyl ether and 1.28 g of oleic acid (4.56 mmol) at 100 °C [1:3 molar ratio of $Fe(CO)_5$ to the oleic acid]. The resulting mixture was heated to reflux (~280 °C) and kept at that temperature for 2 h. During this process, the initial orange color solution turned black, indicative of the presence of Fe^0. When the starting reaction mixture contained $Fe(CO)_5$ and oleic acid in 1:1 and 1:2 molar ratios, nanocrystallites with particle sizes of 5 and 8 nm were obtained, respectively. To produce bigger particles, as for the case of 13-nm nanospheres, a synthesis with a 1:4 molar ratio was used, and then more iron carbonyl $Fe(CO)_5$ was added into the previous colloidal dispersion, followed by aging at temperatures close to 280 °C. The resulting black solution was then cooled to room temperature, and ethanol was added to yield a black precipitate, which was then separated by centrifugation. The supernatant was discarded, and the particles were redispersed in chloroform. This washing sequence was repeated three times to remove surfactant excess from solution. For the solutions containing the slighter particles, warming up the colloidal dispersions from cryogenic temperatures under the presence of a permanent magnet was also complementary to the centrifugation routine.

The reduction reactions during preparation of the different NPs were carried out under Ar atmosphere. Ulterior washing, drying, storage and transfer to transmission electron microscopy (TEM) or superconducting quantum interference device (SQUID) were carried out in ambient conditions.

Electron microscopy experiments were carried out in a LEO 922A energy filtered TEM (EFTEM), operating at 200 kV and a JEOL 2011 high-resolution TEM (HRTEM), operating at 200 kV. Samples were prepared by drying solvent dispersions of NPs onto a lacey C film supported on Cu grids.

Magnetic properties of the samples have been measured using a Quantum Design MPMS-5 SQUID magnetometer in the temperature range from 10 to 300 K and in applied fields up to 50 kOe.

III. RESULTS AND DISCUSSION

A. Structural characterization

Typical low magnification TEM images of the Fe NPs considered in this paper are shown in Fig. 1. Variations in the synthesis procedure engender NPs with average diameter ranging from 5 to 13 nm. The particle size was most sensitive to the surfactant-to-iron molar ratio. The time of reflux was also a determining factor in uniformity of particle shape and size monodispersity. This is normally explained by the formation of an intermediate iron-oleate complex, the time and temperature dependence of the reaction attributed to the decomposition of different intermediates, the concentration of surfactant controlling the nucleation and growth.

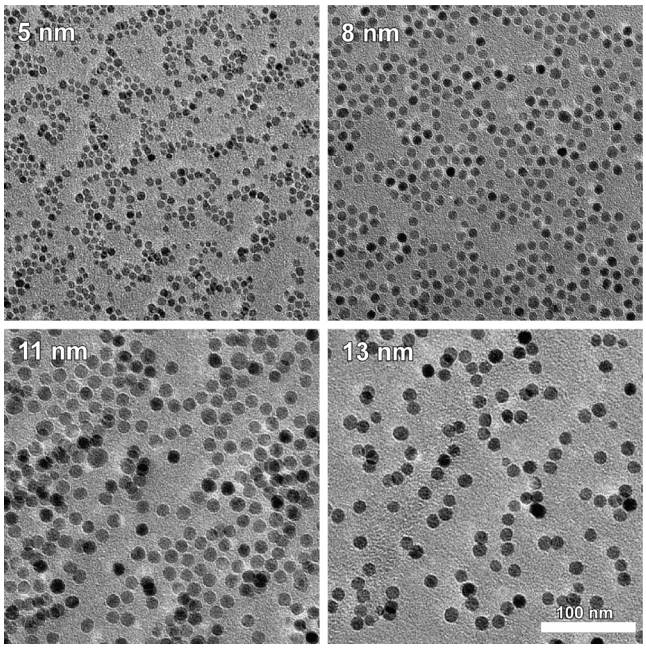

FIG. 1. Low magnification TEM images of several assemblies of spheroidal NPs with average diameter ranging from 5 to 13 nm.

The great contrast variations between the particles indicate randomly oriented single crystals. This is also readily confirmed by the spotty ring selected area diffraction (SAD) pattern in Fig. 2, obtained from a typical area in the sample with 13-nm size particles. Detailed measurements of the observed lattice spacing in the SAD patterns revealed that the great majority of the particles are crystallized in the magne-

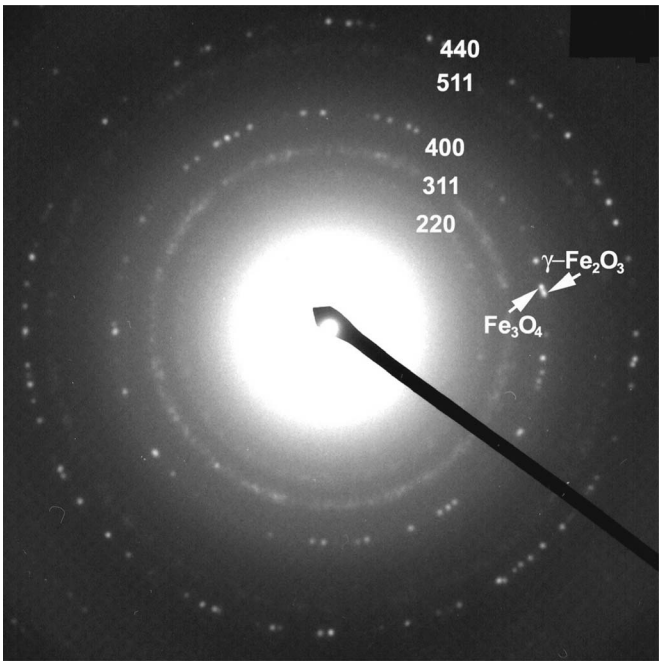

FIG. 2. Typical SAD pattern obtained from the 13-nm NPs. The main diffraction rings are indexed to Fe_3O_4. The co-existence of γ-Fe_2O_3 in the same sample is shown by the double (400) spots, marked with white arrows.

tite (Fe_3O_4) phase; however, in some cases, such as that shown by the white arrows in Fig. 2, individual reflections by both the Fe_3O_4 and the maghemite (γ-Fe_2O_3) phases could be easily revealed.

Variation in contrast between nonoverlapping nanoparticles is due to the different crystallographic orientation of each one with respect to the electron beam.[10] For the same reason in overlapping nanoparticles the contribution of two orientations results in this appearance. Additionally, the contrast variations within each NP arise because lattice fragments are at different orientations with respect to the electron beam. The same type of thickness contrast of spherical or nearly spherical particles has been also previously reported,[11] where metal nanoparticles are shown to have such contrast variations due to their superposition one on top of the others. Finally, it is worth noting that in agreement with relevant works[1,12] the synthesis method of nanoparticles in this manuscript, i.e., the thermal decomposition of iron-organic precursors in an organic media, leads to precipitation of very uniform nanoparticles with low polydispersity.

Although, Mossbauer spectroscopy[13] and x-ray appearance near-edge structure (XANES) (Ref. 14) are quite powerful techniques for the determination of the precise phase in the nanoparticles, detailed HRTEM may also distinguish the magnetite and maghemite phases present as discussed below.

The SAD patterns from various areas of the samples (the representative case presented in Fig. 2) provided only an indication of the co-existence of the oxide phases present in the samples. However, the precise determination of the crystal phase and their relative percentage were performed by means of the Fourier transform (FT) method in each individual nanoparticle, imaged in HRTEM conditions. In more detail, the TEM negatives—where an adequate number of nanoparticles was captured—were initially scanned in a high-resolution scanner and, consequently, the FT was obtained from each individual nanoparticle in the HRTEM image by using Gatan's Digital Micrograph software package. A careful calibration of the reciprocal-lattice spacings measured in FTs by using a Si powder standard sample had been previously performed.

Consequently, the NPs consist of a mixture of γ-Fe_2O_3 and Fe_3O_4 oxides, which have nearly the same spinel crystal structure with only $\sim$1% difference in the cubic lattice constant. While the overall size is well controlled (standard deviations $<$5%), the oxidation process may not be, resulting in homogeneously sized NPs with different ratios of iron and oxygen compounds.

The type of oxide that is formed is an important issue to be pursued. Magnetite is ferrimagnetic below 860 K, with a saturation magnetization value of 84 emu/g, the net magnetization reflecting the Fe^{2+} ions in the octahedral sites. In maghemite the net magnetic moment originates from Fe^{3+} ions, with a magnetic order-disorder transition temperature close to 1020 K and a bulk saturation magnetization of 74 emu/g. Therefore HRTEM and image processing was subsequently employed to reveal the precise crystal structure of individual particles. A typical HRTEM micrograph from the 13-nm sample is displayed in Fig. 3, illustrating the highly crystalline nature of the NPs. Detailed measurements of the reciprocal-lattice spacing by means of FT analysis showed that each individual particle is either in the form of γ-Fe_2O_3 or Fe_3O_4. The magnetite particle exhibits its [110] projection, with the $(2\bar{2}0)$ crystal planes predominately revealed; the particle is also highly facetted at the {111} and {100} planes, in the form of truncated octahedrons as would correspond to entities formed by adatom diffusion close to the thermodynamic equilibrium. The main lattice planes revealed for the maghemite particle are the $(1\bar{1}0)$ and $(11\bar{1})$, as shown in Fig. 3, hence the corresponding zone axis is the [112] in this case.

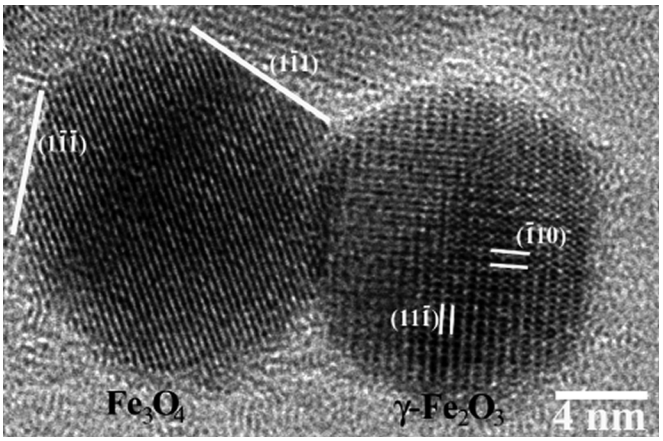

FIG. 3. HRTEM image of two 13-nm-size NPs, each comprised of the two (Fe_3O_4 and γ-Fe_2O_3) different crystal structures. The composition ratio of Fe_3O_4/γ-Fe_2O_3 was found to be 2:1 in that sample.

Eventually, we were able to distinguish the phase (Fe_3O_4 or γ-Fe_2O_3) each individual nanoparticle comprised of and their relative percentage. Furthermore, the FT analysis was quite facilitated in cases where the $\{\underline{1}10\}$ γ-Fe_2O_3 lattice fringes were resolved—e.g., in Fig. 3 of the manuscript—which are only present in maghemite due to the different space group of the two oxide phases.

By measuring more than 100 nanoparticles in each of the two samples (with the 5- and 13-nm particles), we were able to estimate the relative percentage of each phase in them. However, since TEM and HRTEM are sampling techniques and due to the slight lattice spacing variations observed in the nanoparticles, there is indeed an uncertainty in the percentage values for each sample, in the order of about 5%, not capable though to dramatically change the Fe_3O_4/γ-Fe_2O_3 relative ratio in the form of $(\gamma\text{-}Fe_2O_3)_{1-x}(Fe_3O_4)_x$ with $x=0.7$ for the 13-nm sample. The proportion of γ-Fe_2O_3 component gradually increases on decreasing the particle size, reaching $x=0.3$ on the small 5-nm particles.

The structure and oxidation state of the oxide depend on particle size. More precisely, smaller particles are richer in maghemite, while increasing core mean size, the shell becomes mainly composed of magnetite. Due to the reduced radius of curvature, the oxide layer of the smaller particles is expected to exhibit a higher degree of structural disorder and lower coincidence interfaces between crystallites. These features enhance the diffusion of vacancies and Fe cations, thus enhancing the rate of the magnetite to maghemite transformation.[14]

A similar composition dependence on size has been reported by Park *et al.*[15] The origin of the correlation between surface reactivity and particle size may rely on the decay length of the electronic local density of states at the Fermi energy, similar to quantum-size effects observed in the oxidation rate of ultrathin Mg(001) layers on W(110) as a function of film thickness.[16] Bonds to the surfactant chains and the presence of dislocations at the particle surface are factors which are expected to influence the decay length and therefore the electron transfer rate by tunneling, from the metal to the O_2 molecule, which is supposed to control the initial oxidation process. For instance, varying the length of the polymer is believed to explain the different degree of surface oxidation in our case compared to colloidal iron dispersions reported by Griffiths *et al.*[9]

Actually, the oxidation of Fe starts during synthesis due to the presence of an oxygen-containing ligand like oleic acid.[17] Such mechanism leads to surface oxidized nanoparticles at a varied shell depth depending on reflux temperature and duration. Additionally, the use of a solvent such as octyl ether with a high boiling point (287 °C) allows the rearrangement of the atoms within the nanocrystal during the synthesis, giving rise to high crystalline nanoparticles. In addition, we observed that the initially formed oxides have a large Fe/O ratio compared to maghemite and magnetite. We believe that oxidation mainly occurs after exposure in atmosphere following this route: an instant total oxidation of the nanoparticle (all of the measurements presented took place after this stage) and a very slow oxidation of the formed oxides to maghemite (after some months) as shown by x-ray diffraction (XRD) experiments. Finally, the oleic acid (used as a surfactant) seems to be strongly bound to particle surface leading to magnetic isolation and further oxide isolation.

Furthermore, the oleic acid, as a surfactant, containing 18 carbon units, provides spacing between the particles on the order of 3 nm. At these distances, magnetic dipolar interactions are so weak that particles will tend to form two-dimensional arrays. Therefore regular arrays of nanosized magnetic Fe-based particles, separated by the fatty acid molecules adsorbed to their surfaces, can be formed by drying the solution under the appropriate conditions (humidity, temperature, boiling point of the solvent, particle concentration in the solution, etc.) on different kinds of substrates. The choice of the appropriate substrate based on its chemical environment and properties plays crucial role in monodispersity. But also the thermal decomposition as a synthesis method facilitates the self-assembly mechanisms in iron oxides.

Deposition of several metal (Cr, Pt, Al) and semiconductor (Si) capping layers, together with the use of microfabricated wafers, will allow the integration of chemically synthesized NPs from organic solvents into structures suitable for magnetospintronics applications. Up to now, devices were formed from multilayers of superparamagnetic Fe_3O_4 NPs deposited in vertical tunnel junctions using the Langmuir-Blodgett technique,[18] or utilized the nanometer-scale precision of the NP's self-assembly.[19] In our study, a different procedure was followed with very promising results as Fig. 4 depicts. This TEM micrograph was recorded after carefully depositing a drop of the solution onto a silicon substrate by means of spin-coating methods. After the NP's film formation, a conducting 10-nm Cr electrode was evaporated under vacuum conditions. The quality of the monolayered ordering of islands is evident.

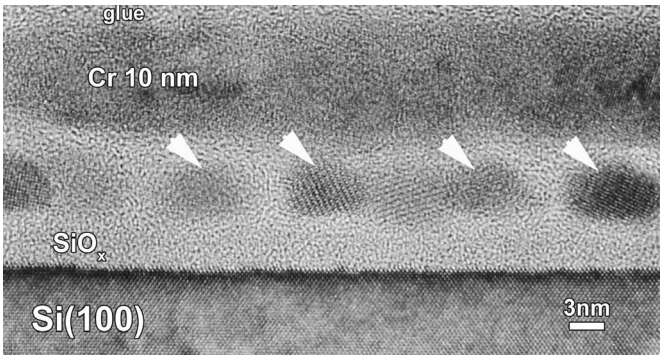

FIG. 4. HRTEM image of 5-nm particles, indicated by arrows, embedded in an organic barrier onto Si(001). In this case, the capping layer was a 10-nm-thick Cr film.

The exact shape of nanoparticles is more obvious in this cross section image. Despite the pressure of the Cr overlayer nanoparticles keep their almost spherical shape. In the case that there are oxide nanoparticles having disklike shape, they would be imaged as rectangular in cross sectional TEM image, whereas such a TEM micrograph, as well as from other areas of the NP's film formation sample, reveal that the particles have a spherical shape. The tendency of metallic cores to form elongated shapes depending on size was observed by HRTEM imaging in Fe nanoparticles[20] contrary to our samples where in all sizes mainly spherical nanoparticles were observed. Therefore we believe that there is not such a great percentage of particles with disklike shapes in the sample to induce an additional shape anisotropy.

B. Magnetic characterization

A discussion of the macroscopic magnetic properties of these high-quality NPs follows. The zero-field-cooled–field-cooled (ZFC-FC) magnetization curves in an applied field of 100 Oe are plotted in Fig. 5 for comparison between the samples with 5, 8, and 13 nm average particle diameter. Both types of curves were measured in the direction of increasing temperature between 10 and 300 K. The ZFC curve exhibits a typical blocking process of an assembly of superparamagnetic particles with a distribution of blocking temperatures. From these temperatures, and assuming a spherical shape of the particles with a mean volume $\langle V \rangle$, extracted from TEM pictures, we could estimate[3] the effective anisotropy constant $K_{\text{eff}} \approx 30 k_B T_B / \langle V \rangle$ where k_B is the Boltzmann constant. The calculated value of the effective anisotropy (see Table I) is comparable with first-order anisotropy γ-Fe_2O_3 (and Fe_3O_4) constant usually reported in NP studies following the typical increase with decreasing particle size. However, it is noticeable that unlike other nanocrystals, in our case the magnetic anisotropy constant does not increase significantly with a reduction in particle size.[5,15]

The superparamagnetic behavior of these samples at temperatures above T_B has been confirmed by plotting the field

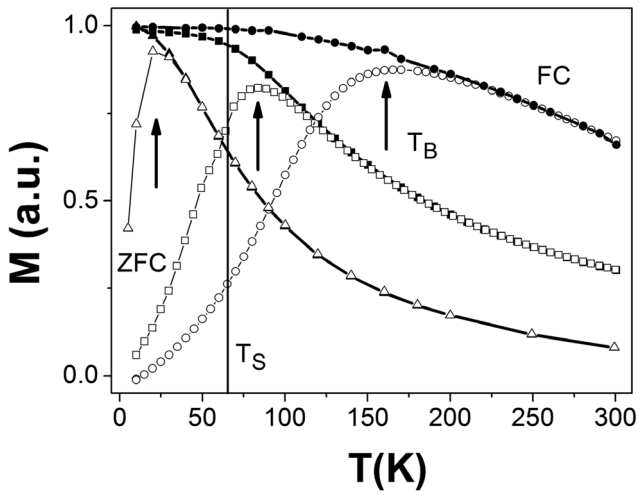

FIG. 5. Magnetization of the 5-nm (triangles), 8-nm (squares), and 13-nm (circles) NPs vs temperature, measured in a field of 100 Oe. The lower curves are for the samples cooled to 10 K in zero magnetic field (ZFC, represented by hollow symbols) while the FC curves are depicted as full symbols. Arrows indicate the blocking temperature T_B for each sample. The vertical line close to 65 K accounts for the surface spin-glass temperature T_s (at which the magnetization deviates from the T^2 dependence).

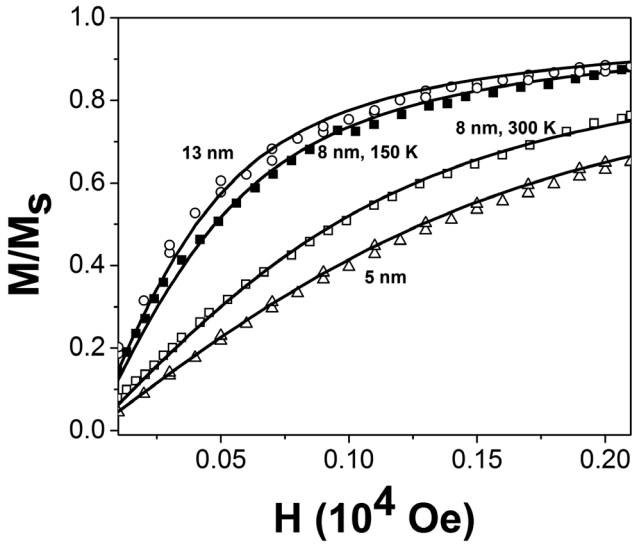

FIG. 6. Isothermal magnetization curves corresponding to the 8-nm particles sample, at 150 K (solid squares) and 300 K (open squares). The magnetization curves for the 13-nm (open circles) and 5-nm (open triangles) samples at 300 K are also shown for comparison. The solid lines are fits to the Langevin expression for a superparamagnet.

dependence of the magnetization as seen in Fig. 6. Considering a system of monodisperse noninteracting particles, it is possible to fit these isothermal magnetization curves to Langevin-like functions $M/M_s = \coth(\mu H/k_B T) - (k_B T/\mu H)$ where μ is the intrinsic magnetic moment of each particle, and T is the temperature.[21] The calculated curves are in good agreement with the experimental data, and the mean magnetic moment per 8-nm particle is found to be $\mu \approx 7785\mu_B$ at 300 K, and about $8414\mu_B$ when measured at 150 K. An estimation of the saturation magnetization can be obtained using the general expression $\mu = M_s\langle V\rangle$. These results correspond to saturation magnetization values of 55 and 59 emu/g, respectively. Here, we have assumed the average density of bulk γ-Fe_2O_3 (4.87 g/cm^3) and Fe_3O_4 (5.2 g/cm^3) phases. It is worthwhile to mention that usually reported values of M_s, for the iron oxide particles case, were found smaller than the bulk value and decreasing even more by reducing the size of the NPs.[1] For comparison, the magnetic saturation of bulk Fe_3O_4 is 84 emu/g, which mainly is that of our 13-nm sized sample. This clearly indicates that the chemical environment (surfactant itself) may be a strong influence on the magnetic properties, together with the spin canting of the surface ions as in the case of ferrimagnetic lattice.[4]

Below T_B the samples show hysteresis in M vs H curves. Figure 7(a) shows the field-cooled magnetic hysteresis loops at 10 K of two representative samples from the series discussed. The hysteresis loop after the field-cooled procedure is shifted along the field axis in the opposite ("negative") direction to the cooling field, i.e., the absolute value of coercive field for decreasing (H_{c1}) and increasing field (H_{c2}) is different. This effect is well known to be due to the exchange coupling between antiferromagnetic AFM (or spin glass) phases and ferromagnetic FM (or ferrimagnetic) phases.[7,22,23] The following details are also worth mentioning. First, the coercivity at each side of the hysteretic branch increases with the particle diameter, and consequently the *exchange bias* defined as $H_{ex} = (H_{c1} + H_{c2})/2$ and depicted in Fig. 7(b). Second, it is well known that in many exchange-biased film systems, H_{ex} depends on the number of measurements, a property often called a *training effect*. As an example, if several consecutive hysteresis loops are measured, the shift of consecutive loops will decrease. Note that such effect is not detected in our case. This is best observed for the 13-nm sample in Fig. 7(a), where first the hysteresis cycle

TABLE I. Samples types and magnetic characterization.

Diameter (nm)	Phase (% of Fe_3O_4)	T_B (K)	T_C (K)	$M_{s,300\ K}$ (emu/g)	K (10^5 erg/cm^3)	H_{ex} (Oe)	H_c (Oe)
13±0.4	70	160	820±40	86	6	105	479
8±0.4		80	770±20	55	13	50	210
5±0.3	30	19	540±20	43	12	0	45

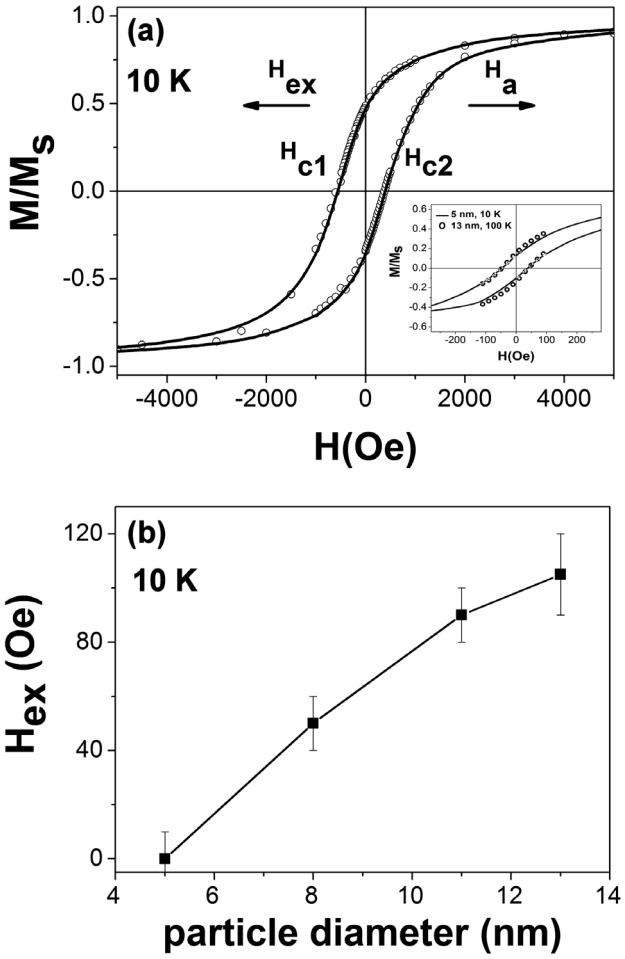

FIG. 7. (a) Normalized magnetization loops for the 13-nm NPs sample at 10 K after cooling from 300 K under an applied field $H_a=+10$ kOe. Circles accounts for the curve measured between ±10 kOe, while the continuous line is the hysteresis measured cycling the field between ±50 kOe. Inset: Hysteresis curves for the 5-nm sample (solid line, measured at 10 K) and the 13-nm NPs sample (circles, measured at 100 K) after FC processes from 300 K down to 10 K under a bias field of +10 kOe. No exchange effects leading to hysteresis displacements are observed. (b) Relation of the exchange field H_{ex}, extracted from the shifts in the hysteresis loops after FC sequences, versus the particle diameter at 10 K. The solid line is a guide for the eyes.

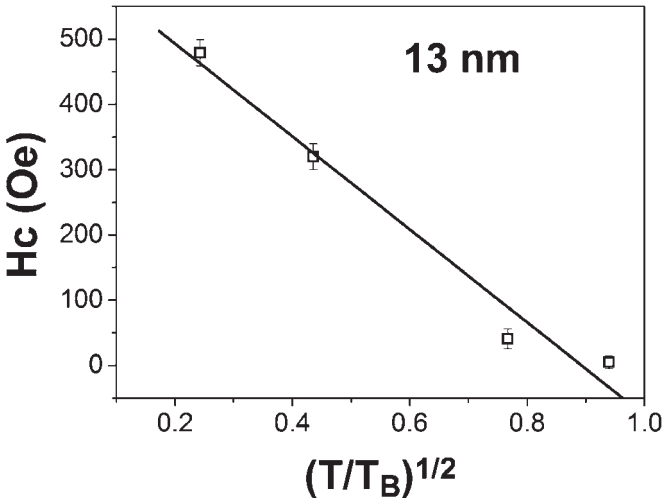

FIG. 8. Example of the coercivity dependence, for the 13-nm sample, as a function of the square root of the temperature normalized to the blocking temperature. The straight line is a linear fit.

was measured between ±10 kOe and then the experiment was repeated under ±50-kOe cycling. This fact suggests the existence in the initial state of a strong local anisotropy, contrasting the orienting action of the applied field. As far as the particle size is concerned, this effect disappears for the sample of 5-nm diameter, the hysteresis curve traced on the inset to Fig. 7(a) being symmetrical without shift.

As the temperature is decreased, the average coercive field $(H_{c2}-H_{c1})/2$ and the remanence increase. For example, at 10 K the value of remanence for the 13-nm particles on Fig. 7(a) is close to the value 0.5 that is expected at 0 K for an ensemble of noninteracting, uniaxial single-domain particles with randomly oriented axis.[2]

The temperature variation of H_{ex} appears below $T\sim 150$ K in correspondence with the freezing point of most moments of the shell regions, indicating that the exchange bias effect originates from the exchange interaction between the cores and the shells. While T reduces, H_{ex} increases because of the progressive freezing of a rising number of shell region moments in agreement with relevant work on iron nanoparticles embedded in an iron oxide matrix.[24]

Neglecting the interparticle correlations and considering that the magnetization reversal process takes place coherently, the coercivity is expected to follow the relation $H_c(T)=H_{c0}[1-(T/T_B)^{1/2}]$. As can be seen in Fig. 8, the extrapolated value of the intrinsic coercive field H_{c0} has been derived to be close to $H_{c0}\approx 670\pm 40$ Oe for the 13-nm sample. H_c increases rapidly with decreasing T, reflecting the freezing of the shell that, because of the exchange coupling, also exerts a strong pinning action against the reversal of the core moments.

In addition, the temperature dependence of the saturation magnetization has, for all the samples, been observed to follow a monotonic decrease different to the Bloch's $T^{3/2}$ law. Figure 9 shows the magnetization of the particles, measured at 20 kOe, as a function of temperature. In our case, $M(T)$ can be well described by a power law $M=M_0(1-bT^{\alpha})$ where $\alpha=2\pm 0.1$ for all the cases considered. Such a behavior was initially predicted by Hendriksen *et al.*,[25] at the nanometer scale, due to finite-size effects, where the spin-wave spectrum is modified and the magnetization is better accounted by a T^a power law, with a Bloch exponent $a\sim 2$ larger than its bulk value $(\frac{3}{2})$. Ever since, this methodology is widely used in literature[26,27] to fit the thermal behavior of various nanoparticle systems. Additionally, the temperature dependence of the saturation magnetization for the ultrafine particles in the present work agrees with theoretical calculations[28] on cubic structured spherical particles where the spin-wave spectrum is quantized due to finite-size effects. By extrapolating to zero magnetization, the Curie temperature (T_C) for the sample 13 nm is estimated to be 820 K. As the particle diameter is decreased, the T_C is expected to deviate from the bulk value,[29] and so we found a reduced

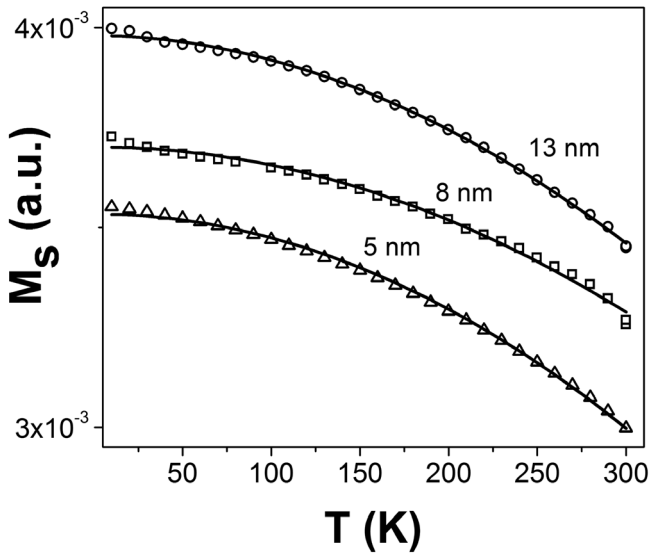

FIG. 9. Magnetization as a function of the temperature for the 5-nm (triangles), 8-nm (squares), and 13-nm (circles) NP solutions. The magnetization was measured in a field of 20 kOe. The solid line shows (fit) the magnetization as a function of T^2.

$T_C \approx 770$ K for the sample with 8-nm average particle diameter and an even more reduced $T_C \approx 540$ K for the 5-nm sample. In Fig. 9 there is also an important increase of the magnetization at low temperatures, which can be understood in terms of a surface state with canted atomic moments. For low temperatures (<50 K) similar increase of magnetization has also been evidenced for ferrite nanoparticles and attributed to misaligned surface spins due to broken exchange bonds. These spins fluctuate more freely at high temperatures than those from the core and freeze progressively at low temperatures into a disordered structure.[30,31] Magnetization vs temperature experiments at different applied fields and particle sizes show that the temperature T_s, at which the magnetization deviates from the previously examined T^2 law, increases from 30 K (measured at 20 kOe cooling field) to 50 K for decreasing fields down to 10 kOe, and extrapolates to $T_s \approx 65 \pm 10$ K for cooling at low fields. For instance, this temperature corresponds with the vertical line in Fig. 5, depicting also the change in the slope of the FC sequences at low field.

The decrease of M_s with decreasing NP size could be explained by considering the presence of a noncollinear magnetic outmost shell of thickness t that relatively increases with decreasing particle size. As the particle size decreases the ratio of thickness of the outer layer to the particle size increases.[26] Similar reduction in magnetization was also observed in ultrafine maghemite particles[32] and ferrite particles[33] and attributed to canting of individual spins, to the presence of a nonmagnetic layer at the particles surface, cation distribution, superparamagnetic relaxation, and spin canting.

IV. DISCUSSION

A necessary condition for the observation of exchange bias is that the antiferromagnetic phase (or ferrimagnetic or spin glass) has a large magnetic anisotropy, so that it can exert a pinning action on the ferromagnetic phase. H_{ex} appears below $T=150$ K in correspondence with the freezing of most of the moments of the oxide magnetic regions, most probably due to the progressive increase of the coercive field, the anisotropy and the consequent freezing of more and more oxide region moments.

We have observed high-field irreversibility in the moment vs temperature of $(\gamma\text{-}Fe_2O_3)_{1-x}(Fe_3O_4)_x$ particles, composition ranging from $x=0.7$ for the 13-nm sample to $x=0.3$ for the 5-nm case. The onset temperature of this irreversibility is near 30 K. The appearance of shifted hysteresis loops leads us to consider a particle as containing a magnetically disordered surface of a certain width and a core more or less ordered depending on the size of the particle and the temperature. The disorder of the spins at the surface of the magnetic NPs could be expected for many reasons. For instance, the surface spins have a lower coordination number and therefore experience a reduced mean field which is sufficient to induce their disorder. Either roughness at the particle edge, the existence of oxygen vacancies at the surface because an inhomogeneous oxidation of the initial Fe colloid, or due to the bonding with the surfactant, would also wane the superexchange interaction, thus inducing the spin-canting effect.[7]

Thermal fluctuations of canted surface spins were also observed in ferromagnetic particles[5,34,35] as well as boundary spins in antiferromagnetic ball-milled FeRh (Ref. 6) and pure nanocrystalline Fe (Ref. 36) have been found to freeze at low temperature into a spin-glass-like phase with a multidegenerate ground state. The origin of this behavior was ascribed to the combination of structural disorder and frustration due to competing magnetic interactions. In our samples, too, the spins of the surface layers could be frozen in a spin-glass-like state at low temperature. Such a picture is supported by the observed high-field irreversibility that appears at hysteresis loops (~ 10 kOe at 5 K for the 13-nm sample). Hence the shift of the field-cooled hysteresis loop can be associated with the exchange anisotropy originating from the exchange coupling between the spin-glass layer and the ferromagnetic cores. At low temperature, the whole system should be in a disordered magnetic state, where the orientation of the layer and the core moments is affected by the exchange coupling between the spin-glass layer and the ferromagnetic phase.

In other words, it can be assumed that the surface layer is characterized by a random magnetic anisotropy (locally varying easy axis and distribution of local anisotropy constant) that increases with decreasing temperature. At high temperature, where the oxide anisotropy is lower, the polarizing action of the cores to the surface moments dominates, and this implies an enhancement degree of the collinearity of the moments.

On this basis we may conveniently describe our system as constituted by two different components, strongly coupled at the interface: a nonrelaxing (quasistatic) ferromagnetic component (core), and a relaxing, magnetically disordered component (surface layer).

At room temperature, most of the net moments of the surface regions thermally fluctuate and tend to be polarized by the core particle moments. Such a description is supported by the magnetization values obtained shown in Table

I. Moreover, spin canting is also a size-dependent feature and we believe that reduced coordination and hence broken superexchange bonds between surface spins result in an alteration of the orientation of each magnetic moment and consequently to a disordered spin configuration and a reduction of the average net moment. With decreasing temperature, a progressive freezing of the moments of the surface layer at field-dependent temperatures occurs, according to the distribution of anisotropy energy barriers. Finally, below a weakly field-dependent temperature T_s, the freezing of the surface layer in a spin-glass-like state is complete and the shell-core exchange coupling results in a frozen disordered magnetic state for the whole system.

In the FC process, a preferred orientation is imposed upon the spin-glass-like surface spins, while the FM core, with a higher ordering temperature, is single domain. When the field is removed, the FM core experiences the field generated by the frozen surface layer in the direction of the cooling field, originating the observation of the offset of the hysteresis loop at measuring temperatures lower than T_s. The disappearance of the exchange bias effect at temperatures over T_s, for instance the 13-nm particles case inserted in Fig. 7(a) while the sample is well below T_B clearly reinforces the above discussion. In addition, if the system undergoes the T_s while the core is still at a superparamagnetic state, as is the case for the sample with particles of 5 nm diameter, the external magnetic field in the FC process cannot select a preferred configuration in the spin-glass-like surface, and a centered hysteresis loop results.

Additionally, one may attribute the disappearance of exchange bias to the decreasing thickness of this spin-glass-like layer when decreasing nanoparticle size. The general trend is that when AFM thickness is reduced, H_{ex} decreases abruptly and finally becomes zero. The exact thickness at which the different stages in this process take place depends on the specific system, microstructure, and the measurement temperature. The decrease of H_{ex} for thin enough layers is due to several connected factors. It is well known that exchange bias requires the condition $K_{AFM}t_{AFM} \geqslant J_{int}$ to be fulfilled. Thus as t_{AFM} is reduced this condition is violated, moreover, the dependence of K_{AFM} with AFM thickness, may also influence H_{ex}. Another important factor is the thickness dependence of T_N and thus the blocking temperature T_B of the AFM layer. Therefore for thin enough layers the reduced temperature varies with thickness. In various systems there is a peak in H_{ex} before the main decrease, a behavior predicted theoretically if there is a change in the AFM domain structure with decreasing thickness. Such a behavior was observed by Berkowitz *et al.*[37] The multisublattice spin configuration considered, in which the reduced coordination of surface spins causes a fundamental change in the magnetic order throughout the particle leading to significant moments which further increased with decreasing average particle diameter is contrary to our samples as shown in Table I. The large contribution of the orbital part of the magnetic moment exhibited in CoO nanoparticles[38] due to a large spin-orbit coupling may eventually cancel the core-shell structure and diminish the exchange bias effect by causing a change in the magnetic ordering in the core of the nanoparticles. However, only x-ray magnetic circular dichroism (XMCD) experiments at Fe, O edges will clarify this issue by determining the L_z/S_z ratio.

The exact nature of the exchange biaslike properties dependence on particle size is presently unclear. At least three types of fundamental processes need to be taken into consideration in this system.

The first is the thermal fluctuations on the superparamagnetic core with decreasing NPs diameter, already discussed, which may destroy the freezing of the surface moments through indirect exchange interactions for the case $T_s < T_B$.

In this case the completely frozen state evolves into a regime where the oxide magnetic regions become progressively unfrozen, according to the distribution of the effective anisotropy energy barriers, determined by their size and by the strength of the magnetic interaction with the surrounding. Once the net moments of the surface layer become able to thermally fluctuate, they tend to be polarized by the core moment. Numerical calculations of the exchange bias in core-shell magnetic nanoparticles[39] predict that the exchange bias is due entirely to the existence of the FM/AFM interface and depends on the structure of the interface and less on its size. Consequently, the influence of the thermal fluctuations on the interface will depend on the shell thickness requiring at least two or more AFM layers to stabilize the exchange bias field.

The second is the chemically dependent surface anisotropy. From the hysteresis shift, we may treat this surface anisotropy as uniaxial, with the easy axis defined by the dipole moment of the neighboring ions. Hence the easy axis for these ions is approximately radial. Therefore if the spins were perfectly aligned, the effect of a radially symmetric surface anisotropy would average to zero. On the one hand, it would appear that this type of irreversibility would not occur if all the cations had the same moment, like in the case of γ-Fe_2O_3 which only contains Fe^{3+} ions, and indeed we do not observe hysteresis shift in samples with 5-nm-diameter particles and a predominant γ-Fe_2O_3 nature. Although Martínez *et al.*[5] studies in the ferrimagnetic oxide γ-Fe_2O_3 as a function of the particle size indicate that the effects become larger as the particle diameter decreases, as expected from a surface effect, we must recall here that in their case the NPs were platelets with an aspect ratio close to 4, which gives a very large specific surface area but departing from the radial symmetry previously discussed. On the other hand, we cannot completely exclude the presence of a certain amount of a nonstoichiometric Fe_xO (wüstite) phase in the NP's surface. Wüstite is paramagnetic at room temperature and antiferromagnetic below 183 K. Since Fe_xO can be oxidized to magnetite, we may expect a relative amount of Fe_xO at the surface of Fe_3O_4 particles. As the amount of Fe_3O_4 in solution increases with the particles diameter, an increase of the magnetic exchange coupling, caused by interfaces between antiferromagnetic Fe_xO and the ferrimagnetic Fe_3O_4, would be anticipated. But the centered hysteresis loop for the 13-nm NPs at 100 K in the inset to Fig. 7(a), while the sample is well below the antiferromagnetic ordering temperature for Fe_xO, clearly declines the above discussion.

And the third, energy competition could be relevant since in small particles the exchange energy, a surface term, becomes larger than the Zeeman energy, a volume energy term,

which tends to orient the surface spins along the field direction. In this sense, coupling for an AFM/FM sandwich has been introduced into a phenomenological free energy expression by Meiklejohn and Bean. It can be shown that in the limit of infinite anisotropy of the antiferromagnet, the hysteresis loop will shift by an amount $H_{ex}=J_{int}/M_{FM}t_{FM}$ along the magnetic-field axis. The formula exhibits the well-known dependencies of exchange on the FM layer thickness t_{FM}, on the magnetization M_{FM}, and on the exchange coupling constant at the interface J_{int}. The AFM magnetization is generally assumed to be zero. However, this is no longer the case in NPs with a spin-glass layer. Within a generalized Meiklejohn-Bean model,[40] the exchange bias is then calculated according to $H_{ex}\sim(a/t_{FM})+(b/t^2\text{AFM})$. Identifying the t_{AFM} with the spin-glass layer, a peak function in the H_{ex} vs the particle size may be observed due to changes in the AFM domain structure.[37] Such transition determines a critical diameter for spheroidal NPs below which the spin disorder is not favorable, and consequently the surface moments should be aligned with the core moments under the application of an external field.

V. CONCLUSIONS

Detailed structural and magnetic study of naturally oxidized iron nanoparticles were presented in this work. Finite-size effects seem to be responsible for the macroscopic magnetic behavior of the nanoparticles' assembly. In particular, magnetic features like the blocking temperature, the Curie temperature, the anisotropy constant, and the saturation magnetization were found to be correlated to the nanoparticle size and the γ-Fe_2O_3/Fe_3O_4 ratio.

Critical radius for exchange bias was evidenced together with high-field irreversibility and attributed to a low-temperature surface spin-glass layer. Hence these effects are associated with exchange anisotropy originating from exchange coupling between spin-glass layer (shell) and the ferromagnetic core. The phenomenon of surface spin glass is strongly dependent on the particle size and diminishes when decreasing the particle diameter. As far as the particle size is concerned, this effect disappears for the sample of 5-nm diameter.

In addition, we have shown that regular arrays of nanosized magnetic Fe-based particles can be formed by spin coating the solution under the appropriate conditions. This may allow the integration of chemically synthesized NPs from hydrocarbon solvents into structures compatible with Si technologies for electronic transport measurements. Further work will aim to explore the magnetotransport behavior of the samples, for instance, quantum tunneling from ferromagnetic electrodes through 3-nm organic barriers and single-electron-transistor effects.

ACKNOWLEDGMENTS

This work was supported by the Marie Curie Research Training Network *SyntOrbMag* (Contract No. MRTN-CT-2004-005567). We would like to thank Ll. Balcells and J. Tsiaoussis for stimulating discussions.

[1] D. L. Huber, Small **1**(5), 482 (2005).
[2] E. C. Stoner and E. P. Wohlfarth, Philos. Trans. R. Soc. London, Ser. A **240**, 599 (1948).
[3] L. Néel, Ann. Geophys. (C.N.R.S.) **5**, 99 (1949).
[4] J. M. D. Coey, Phys. Rev. Lett. **27**, 1140 (1971).
[5] B. Martínez, X. Obradors, Ll. Balcells, A. Rouanet, and C. Monty, Phys. Rev. Lett. **80**, 181 (1998).
[6] A. Hernando, E. Navarro, M. Multigner, A. R. Yavari, D. Fiorani, M. Rosenberg, G. Filoti, and R. Caciuffo, Phys. Rev. B **58**, 5181 (1998).
[7] R. H. Kodama and A. E. Berkowitz, Phys. Rev. B **59**, 6321 (1999).
[8] V. Skumryev, S. Stoyanov, Y. Zhang, G. Hadjipanayis, D. Givord, and J. Nogués, Nature (London) **423**, 850 (2003).
[9] C. H. Griffiths, M. P. O'Horo, and T. W. Smith, J. Appl. Phys. **50**, 7108 (1979).
[10] C. B. Murray, Sh. Sun, W. Gaschler, H. Doyle, T. A. Betley, and C. R. Kagan, IBM J. Res. Dev. **45**, 47 (2001).
[11] A. Wellner, P. Brown, C. J. Kiely, and J. P. Wilcoxon, Inst. Phys. Conf. Ser. **161**, 561 (1999).
[12] A. G. Roca, M. P. Morales, K. O'Grady, and C. J. Sierna, Nanotechnology **17**, 2783 (2006).
[13] C. R. Alves, R. Aquino, J. Depeyrot, T. A. P. Cotta, M. H. Sousa, F. A. Tourinho, H. R. Rechenberg, and G. F. Goya, J. Appl. Phys. **99**, 08M905 (2006).
[14] L. Signorini, L. Pasquini, L. Savini, R. Carboni, F. Bocherini, E. Bonetti, A. Giglia, M. Peddio, N. Mahne, and S. Nannarone, Phys. Rev. B **68**, 195423 (2005).
[15] J. Park, K. An, Y. Hwang, J.-G. Park, H.-J. Noh, J.-Y. Kim, J.-H. Park, N.-M. Hwang, and T. Hyeon, Nat. Mater. **3**, 891 (2004).
[16] N. Binggeli and M. Altarelli, Phys. Rev. Lett. **96**, 036805 (2006).
[17] D. Farrell, S. A. Majetich, and J. P. Wilcoxon, J. Phys. Chem. B **107**, 11022 (2003).
[18] P. Poddar, T. Fried, and G. Markovich, Phys. Rev. B **65**, 172405 (2002).
[19] H. Zeng, C. T. Black, R. L. Sandstrom, P. M. Rice, C. B. Murray, and S. Sun, Phys. Rev. B **73**, 020402(R) (2006).
[20] L. Del. Bianco, D. Fiorani, A. M. Testa, E. Bonetti, L. Savini, and S. Signoretti, Phys. Rev. B **66**, 174418 (2002).
[21] A. H. Morrish, *The Physical Principles of Magnetism* (Wiley, New York, 1965).
[22] J. Nogués and I. K. Schuller, J. Magn. Magn. Mater. **192**, 203 (1999).
[23] J. Nogués, J. Sort, V. Langlais, V. Skumryev, S. Suripach, J. S. Mupoz, and M. D. Baró, Phys. Rep. **422**, 65 (2005).
[24] L. Del Bianco, D. Fiorani, A. M. Testa, E. Bonetti, and L. Signorini, Phys. Rev. B **70**, 052401 (2004).
[25] P. V. Hendriksen, S. Linderoth, and P.-A. Lindgård, J. Phys.: Condens. Matter **5**, 5675 (1993).
[26] S. Roy, I. Dubenko, D. D. Edoth, and N. Ali, J. Appl. Phys. **96**,

1202 (2004).
[27] C. R. Alves, R. Aquino, M. H. Sousa, H. R. Rechenberg, G. F. Goya, F. A. Tourinho, and J. Depeyrot, J. Metastable Nanocryst. Mater. **20–21**, 694 (2004).
[28] P. V. Hendriksen, S. Linderoth, and P.-A. Lindgård, Phys. Rev. B **48**, 7259 (1993).
[29] C. M. Schneider, P. Bressler, P. Schuster, J. Kirschner, J. J. de Miguel, and R. Miranda, Phys. Rev. Lett. **64**, 1059 (1990).
[30] F. Gazeau, E. Dubois, M. Hennion, R. Perzynski, and Yu. Raikher, Europhys. Lett. **40**, 575 (1997).
[31] J. L. Dormann, F. D'Orazio, F. Lucari, E. Tronc, P. Prené, J. P. Jolivet, D. Fioranni, R. Cherkaoui, and M. Noguès, Phys. Rev. B **53**, 14291 (1996).
[32] P. V. Hendriksen, S. Linderoth, C. A. Oxborrow, and S. Morup, J. Phys.: Condens. Matter **6**, 3091 (1994).
[33] R. N. Panda, N. S. Gajbhiye, and G. Balaji, J. Alloys Compd. **326**, 50 (2003).
[34] H. Kodama, A. E. Berkowitz, E. J. McNiff, Jr., and S. Foner, Phys. Rev. Lett. **77**, 394 (1996).
[35] E. Tronc, A. Ezzir, R. Cherkaoui, C. Chanéac, M. Noguès, H. Kachkachi, D. Fiorani, A. M. Testa, J. M. Grenèche, and J. P. Jolivet, J. Magn. Magn. Mater. **221**, 63 (2000).
[36] E. Bonetti, L. Del Bianco, D. Fiorani, D. Rinaldi, R. Caciuffo, and A. Hernando, Phys. Rev. Lett. **83**, 2829 (1999).
[37] A. E. Berkowitz, R. H. Kodama, S. A. Makhloul, F. T. Parker, F. E. Spada, E. J. McNiff Jr., and S. Foner, J. Magn. Magn. Mater. **196–197**, 591 (1999).
[38] C. F. J. Flipse, C. B. Rouwelaar, and F. M. F. de Groot, Eur. Phys. J. D **9**, 479 (1999).
[39] E. Eftaxias and K. N. Trohidou, Phys. Rev. B **71**, 134406 (2005).
[40] Ch. Binek, A. Hochstrat, and W. Kleeman, J. Magn. Magn. Mater. **234**, 353 (2001).